

The compact, time-variable radio source projected inside W3(OH): Evidence for a Photoevaporated Disk?

Sergio A. Dzib¹, Carolina Rodríguez-Garza¹, Luis F. Rodríguez^{1,2}, Stan E. Kurtz¹, Laurent Loinard¹, Luis A. Zapata¹, and Susana Lizano¹

s.dzib@crya.unam.mx

Received _____; accepted _____

arXiv:1306.1577v1 [astro-ph.SR] 6 Jun 2013

¹Centro de Radioastronomía y Astrofísica, Universidad Nacional Autónoma de México, Morelia 58089, México

²Astronomy Department, Faculty of Science, King Abdulaziz University, P.O. Box 80203, Jeddah 21589, Saudi Arabia

ABSTRACT

We present new Karl G. Jansky Very Large Array observations of the compact ($\sim 0''.05$), time-variable radio source projected near the center of the ultracompact HII region W3(OH). The analysis of our new data as well as of VLA archival observations confirms the variability of the source on timescales of years and for a given epoch indicates a spectral index of $\alpha = 1.3 \pm 0.3$ ($S_\nu \propto \nu^\alpha$). This spectral index and the brightness temperature of the source ($\sim 6,500$ K) suggest that we are most probably detecting partially optically thick free-free radiation. The radio source is probably associated with the ionizing star of W3(OH), but an interpretation in terms of an ionized stellar wind fails because the detected flux densities are orders of magnitude larger than expected. We discuss several scenarios and tentatively propose that the radio emission could arise in a static ionized atmosphere around a fossil photoevaporated disk.

Subject headings: accretion disks — ISM:individual objects (W3(OH)) — HII regions — radio continuum:stars

1. Introduction

Recently formed massive stars produce large amounts of UV photons that ionize the natal material around them, forming H II regions of different morphologies and sizes. Ultracompact H II (UCHII) regions are small (diameters no more than ~ 0.1 pc) and dense (electron densities of at least 10^4 cm³) volumes of ionized gas produced by one or several massive stars (Wood & Churchwell 1989). W3(OH) is a limb-brightened UCHII region with a shell morphology (Dreher & Welch 1981) that is known to be expanding at a velocity of $\sim 3\text{--}5$ km s⁻¹ (Kawamura & Masson 1998). It is located at a distance of 2.04 kpc (Hachisuka et al. 2006) and the total luminosity of the system is $7.1 \times 10^4 L_{\odot}$ (Hirsch et al. 2012). The region is heavily obscured ($A_V \sim 75$; Feigelson & Townsley 2008) and there is little direct information on the nature of the ionizing star.

Kawamura & Masson (1998), based on the residual image obtained subtracting maps of different epochs, reported a compact, time evolving (over a scale of several years) source projected near the center of W3(OH) and suggested that it is probably related to the central star. Remarkably, no further research has been published since then on this interesting radio source. Here, we report new radio observations of the W3(OH) region made with the Karl G. Jansky Very Large Array (VLA) of the NRAO¹. We also used VLA archive observations to complement our study. Our results provide for the first time a direct radio detection and a determination of the parameters of this radio source, possibly associated with the star that ionizes the W3(OH) region.

¹The National Radio Astronomy Observatory is operated by Associated Universities Inc. under cooperative agreement with the National Science Foundation.

2. Radio Observations

The observations were made in the Ka band (26.5 – 40 GHz) with the VLA centered at a frequency of 32.96 GHz and with a total bandwidth of 2 GHz. The observations were made on 2012 October 13, with the VLA in the A configuration.

At the beginning of the observations we integrated on the standard flux calibrator 3C 48 for ~ 3 minutes. This source was also used as the bandpass calibrator. We then spent one minute on the phase calibrator J0244+6228 followed by five minutes on the target; this cycle was repeated until one hour was completed. The angular distance between the phase calibrator and the target is 2.17 degrees. Referenced pointing scans at the lower frequency of 9.0 GHz were performed before the beginning of the observation of the flux calibrator and before the start of the phase calibrator–target cycle. These scans are required to assure that the absolute pointing of the antennas is accurate to $5''$ or better.

The data were edited, calibrated and imaged in the standard fashion using the Common Astronomy Software Applications package (CASA). After the initial calibration, the visibilities were self-calibrated and imaged with a pixel size of 0.01 arcsecond. The weighting scheme used was intermediate between natural and uniform (WEIGHTING='briggs' with ROBUST=0.0 in CASA). To minimize the extended emission from the H II region we removed the short spacings generated by baselines below 10 km, suppressing angular structures larger than $\sim 0''.2$. The uv range was chosen to provide an optimal compromise between suppressing extended emission and maintaining signal-to-noise and image quality in the resulting maps. The rms noise level of an image processed in this manner depends on the position considered. In the central part of the final images it was around $50 \mu\text{Jy beam}^{-1}$, while in the immediate surroundings of the compact source it reached about $380 \mu\text{Jy beam}^{-1}$.

2.1. Position and Angular Size of the Compact Radio Source

A compact radio source was clearly detected at a position of $\alpha(2000)=02^{\text{h}}27^{\text{m}}03^{\text{s}}867$, $\delta(2000)=61^{\circ}52'24''.89$ (see Figure 1). The source is projected well inside W3(OH) and its total integrated flux density at 32.96 GHz is 14.4 ± 1.0 mJy with a peak of 6.0 ± 0.4 mJy beam⁻¹. Its deconvolved angular size is $0''.05 \pm 0''.01$, implying a physical size of 100 ± 20 AU and a peak brightness temperature of $T_B = 6,500 \pm 2,600$ K. This brightness temperature suggests that we are observing optically-thick photoionized gas. Assuming that the brightness temperature equals the electron temperature of the gas and using the usual formulation for the parameters of a homogeneous HII region (Schraml & Mezger 1969) we can set lower limits to the electron density, $n_e \geq 1.9 \times 10^6$ cm⁻³, ionized mass, $M_{\text{HII}} \geq 9.5 \times 10^{-6} M_{\odot}$, and ionizing photon rate required by the compact source, $N_i \geq 7.8 \times 10^{45}$ s⁻¹. This photon rate is equivalent to that provided by a B1 or earlier ZAMS star. There is marginal evidence in the image of a very faint, extended halo but observations of higher signal-to-noise ratio are needed to test its reality.

In Figure 1 we also show the extent of W3(OH) as observed at 8.4 GHz. These data were taken from the VLA archive and are the average of observations made in the A configuration during 1995 July 04 (under project AR341) and 1996 November 15 (under project AR363). We will refer to these averaged 8.4 GHz data as having a mean epoch of 1996.19. These archive data have been discussed and published by Wilner et al. (1999).

We have also compared the position of the compact radio source with that of the UCHII region W3(OH), as traced in the 890 μm data taken with the Submillimeter Array (SMA)²

²The Submillimeter Array (SMA) is a joint project between the Smithsonian Astrophysical Observatory and the Academia Sinica Institute of Astronomy and Astrophysics and is funded by the Smithsonian Institution and the Academia Sinica.

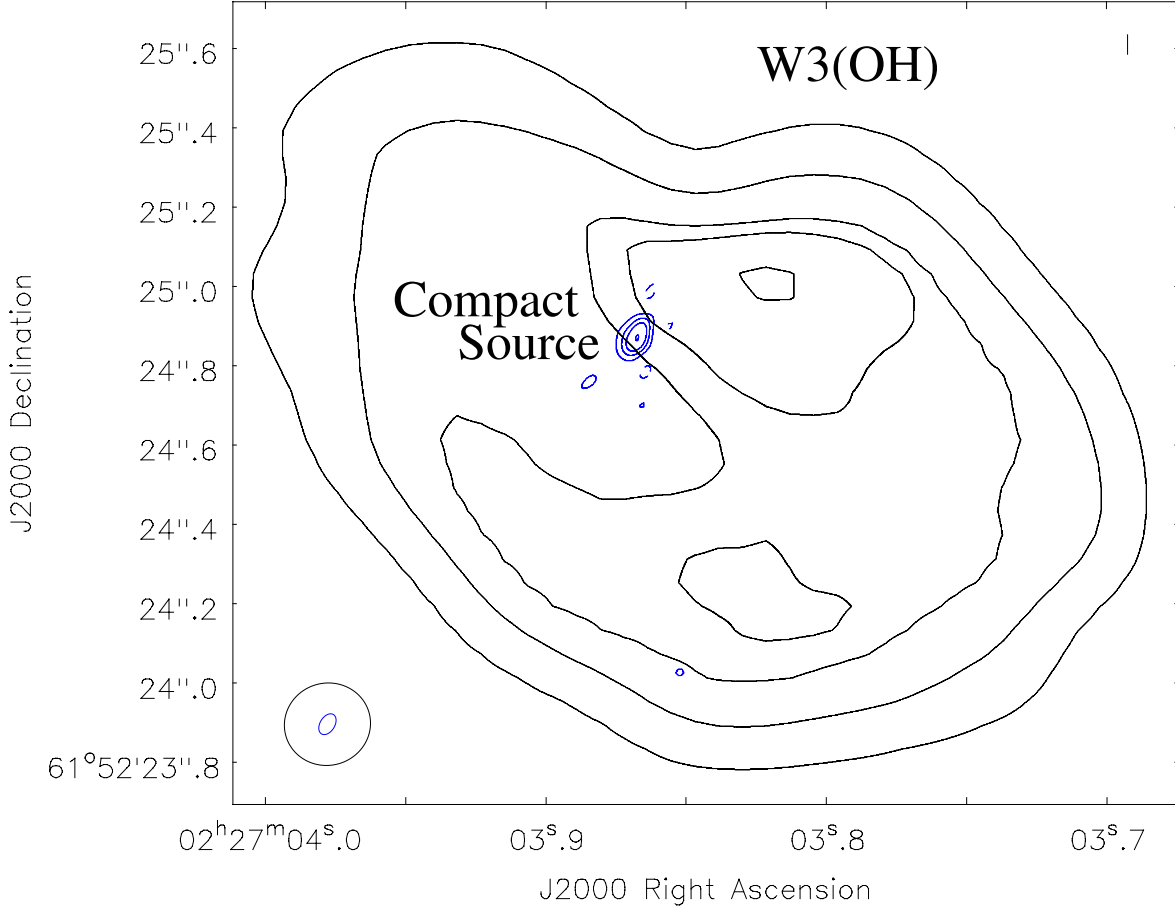


Fig. 1.— Image of the I Stokes parameter of the compact radio source in W3(OH), given in blue contours, as detected in our Ka band (32.96 GHz) observations. The contours are at $-3, 3, 6, 9,$ and 15 times the $1\text{-}\sigma$ noise level of $380 \mu\text{Jy beam}^{-1}$. The black contours delineate the W3(OH) region as observed at a frequency of 8.4 GHz. The contours are at 320, 1000, 1500, 1600, and 1750 times the $1\text{-}\sigma$ noise level of this image ($22 \mu\text{Jy beam}^{-1}$). The half power contours of the 32.96 ($0''.057 \times 0''.037; PA = 148^\circ$) and 8.4 GHz synthesized beams ($0''.218 \times 0''.207; PA = 105^\circ$) are shown in the bottom left corner.

and discussed by Zapata et al. (2011). The total emission of W3(OH) at this wavelength is determined to be 1.8 ± 0.1 Jy and the image is shown in Figure 2. The compact radio

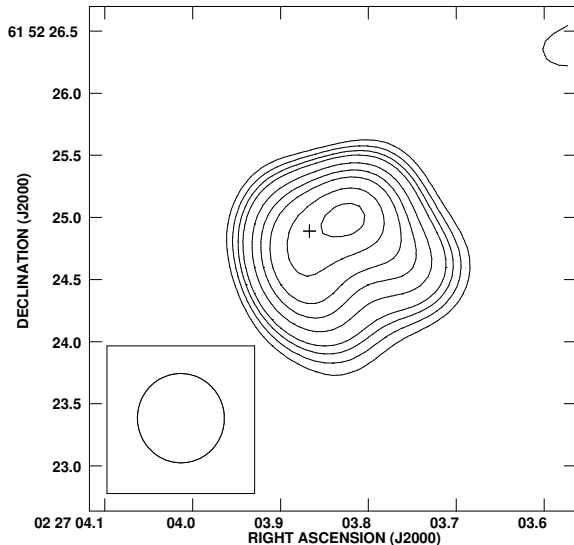


Fig. 2.— SMA 890 μm continuum emission from W3(OH). The contours are at -3, 3, 4, 5, 6, 8, 10, 12, 15, and 18 times the $1\text{-}\sigma$ noise level of 36 mJy beam^{-1} . The half power contour of the synthesized beam ($0''.72 \times 0''.70$; $PA = 5^\circ$) is shown in the bottom left corner. The position of the compact radio source is marked with a cross.

source falls near the centroid of the 890 μm emission. There is an offset of $\sim 0''.3$ between the centroids of the compact radio source and the SMA submillimeter emission. However, the positional accuracy of the submillimeter emission is $\sim 0''.2$ (Cowie et al. 2009) and we cannot attribute significance to this offset.

2.2. Detection of the H58 α line

The Ka band observations were made centered at 32.96 GHz with a total bandwidth of 2 GHz distributed in 1024 individual channels of 1.95 MHz each (equivalent to an average velocity width of 17.8 km s^{-1}). This frequency coverage includes the H58 α radio recombination line, that has a rest frequency of 32.85220 GHz. We analyzed the part of the spectrum where this line was expected and a feature was detected (Figure 3). This line

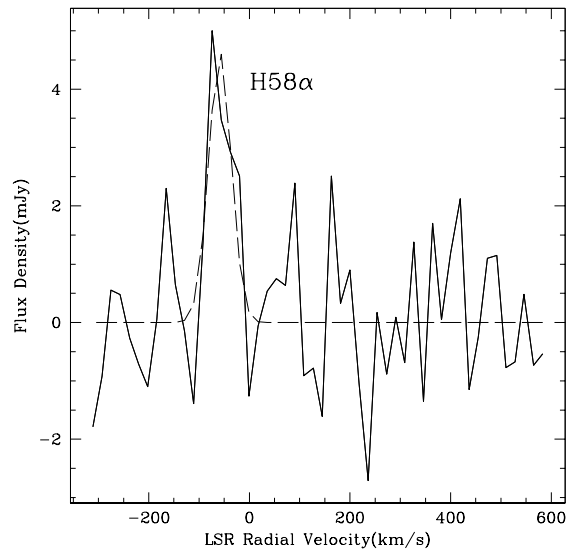


Fig. 3.— $H58\alpha$ emission from the compact radio source in W3(OH). The dashed line is the least-squares fit to the spectrum.

was least-squares fitted with a Gaussian profile, obtaining a peak line flux density of $S_L = 4.6 \pm 1.0$ mJy, a full width at half maximum of $\Delta v = 52.9 \pm 13.1$ km s⁻¹, and an LSR radial velocity of $v_{LSR} = -58.5 \pm 5.6$ km s⁻¹. The analysis was made in the spectral cube obtained without short spacings and in the solid angle containing the compact radio source, with a continuum flux density of $S_C = 14.4 \pm 1.0$ mJy.

We believe that this line corresponds to emission from the compact radio source by two reasons. The first is that the v_{LSR} of the line falls in the range of LSR radial velocities reported for radio recombination lines originating in the UCHII region W3(OH) (-63.5 to -50.3 km s⁻¹; Sams et al. 1996). The second reason is that the observed flux density for the line is in agreement with the expected value. Using the formulation of Rodríguez et al. (2009) for radio recombination lines from an ionized wind in local thermodynamic equilibrium, we expect a value of $S_L = 3.9$ mJy, consistent with the observed value of

4.6 ± 1.0 mJy.

2.3. Spectral Index

We used the VLA archive deep observations of W3(OH), previously reported by Kawamura & Masson (1998, see their paper for a detailed description of the observations) made in the years 1986, 1990 and 1995. We removed short spacings generated by baselines below 8 km. The source is detected in the three epochs (see Table 1). It is strongly variable on a timescale of years, showing minima in 1990 and 1995 and rising again to its 1986 levels in our 2012 observations. Even when the observations are made at different frequencies, it is clear that the flux densities of 1990 and 1995 represent minima with respect to the other epochs after correcting for the spectral index determined from the 1986 observations (see below). Its flux densities for 1986, 1990 and 1995 are consistent with the negative values reported by Kawamura & Masson (1998) in their residual difference maps.

In the epoch 1986.38 the source was detected at the two observed frequencies, allowing us to determine a spectral index of $\alpha = 1.3 \pm 0.3$ ($S_\nu \propto \nu^\alpha$) for this epoch. This spectral index is similar to the one reported for the compact radio source at the center of the H II region NGC 6334E ($\alpha = 1.0 \pm 0.7$), that Carral et al. (2002) interpreted as produced by a stellar ionized wind. We also imaged the Stokes V parameter in all the epochs and detected no circular polarization at levels of $\sim 1 - 10\%$ (4σ upper limits). The long timescale variability, along with the lack of polarization, the positive spectral index, the possible presence of recombination line emission, and the brightness temperature of $\sim 10^4$ K favor optically thick free-free as the emission process. Gyrosynchrotron radiation from a magnetically active young star of low mass would likely be variable on short timescales (hours), show some degree of circular polarization, have a negative spectral index and a high ($\sim 10^7$ K) brightness temperature (e.g. Dzib et al. 2011; Torres et al. 2012).

Table 1: Position, flux density and observed frequency of the compact radio source in the different epochs.

	α (J2000.0)	σ_α	δ (J2000.0)	σ_δ	F_ν	ν
Epoch	$2^{\text{h}}27^{\text{m}}$	(seconds)	$+61^\circ52'$	(arcseconds)	(mJy)	(GHz)
1986.38	03.8709	0.0002	24.919	0.003	09.1 ± 0.5	14.99
1986.38	03.8707	0.0002	24.906	0.003	15.6 ± 1.3	22.46
1990.19	03.8770	0.0004	24.953	0.005	03.8 ± 0.4	14.94
1995.48	03.8707	0.0003	24.890	0.005	02.6 ± 0.2	14.94
2012.78	03.8670	0.0001	24.887	0.002	14.4 ± 1.0	32.92

3. Discussion

3.1. Proper Motions

In our analysis of the available data we have used the improved positions for the phase calibrators available in the VLA Calibrator Manual. This procedure permits absolute systematic errors in the range of $\sim 0''.01 - 0''.02$ (e.g. Gómez et al. 2005). With the positions presented in Table 1, we determine the proper motion of the compact radio source to be ³:

$$\begin{aligned}\mu_\alpha \cos \delta &= -2.3 \pm 0.6 \text{ mas yr}^{-1} \\ \mu_\delta &= -1.1 \pm 0.7 \text{ mas yr}^{-1}.\end{aligned}$$

Systematic contributions of $0''.010$ and $0''.011$ in the α and δ positions, respectively, were

³We do not include epoch 1990.19 in our proper motion analysis because its position does not follow the trend presented by the others, with a difference of $\sim 0''.05$.

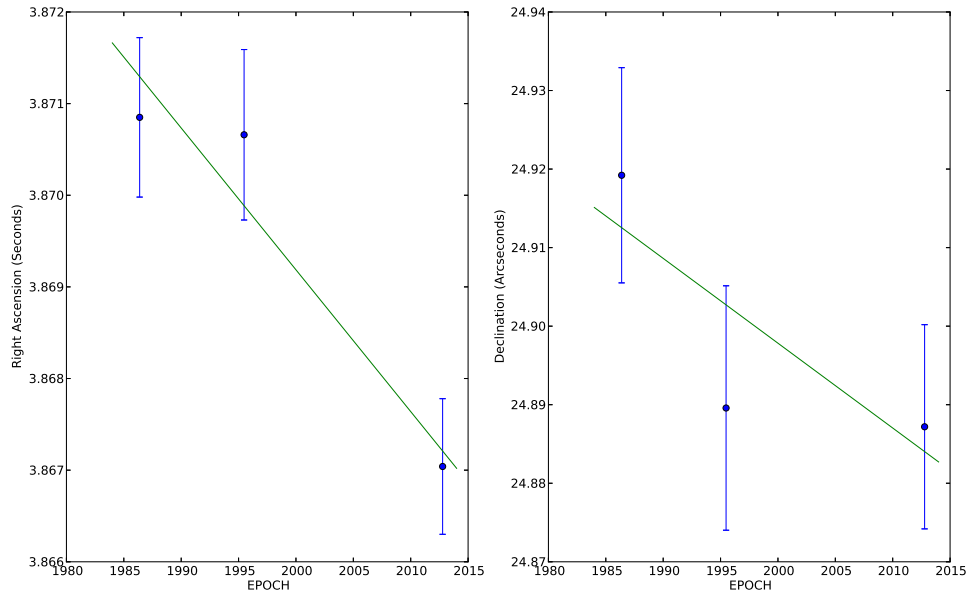


Fig. 4.— Positions of the compact radio source as a function of epoch. The solid lines are the least squares best fits to the positions.

added in quadrature to the positional errors obtained from a Gaussian fit (task IMFIT in CASA), in order to obtain a χ^2 of 1. The positions as a function of the epoch are presented in Figure 4.

Does this proper motion have any significance with respect to the nature of the source? To estimate the characteristic proper motion of the region we compared our 2012 observations with those made at 8.4 GHz for epoch 1996.19 for the TW sources A and C (Turner & Welch 1984; Reid et al. 1995), located about $7''$ to the east of W3(OH). As can be seen in Figure 5, there is a small displacement to the west for the more recent data. TW-A is extended in the east-west direction and not adequate for a proper motion determination that requires sources as compact as possible. Fortunately, TW-C is very compact and for it we estimate a proper motion of

$$\begin{aligned}\mu_\alpha \cos \delta &= -2.7 \pm 0.3 \text{ mas yr}^{-1} \\ \mu_\delta &= -0.3 \pm 0.3 \text{ mas yr}^{-1}.\end{aligned}$$

These proper motions are consistent with those found for the compact radio source and suggest that we are simply observing the secular proper motions of the region. From VLBA observations, Xu et al. (2006) measure a mean proper motion of

$$\begin{aligned}\mu_\alpha \cos \delta &= -1.20 \pm 0.02 \text{ mas yr}^{-1} \\ \mu_\delta &= -0.15 \pm 0.01 \text{ mas yr}^{-1}.\end{aligned}$$

for methanol masers associated with W3(OH). To obtain the expected galactic proper motions we used the galactic rotation model of Brand & Blitz (1993) and the velocity of the Sun with respect to the local standard of rest from Schönrich et al. (2010). We obtain:

$$\begin{aligned}\mu_\alpha \cos \delta &= -0.8 \pm 1.0 \text{ mas yr}^{-1} \\ \mu_\delta &= -0.4 \pm 1.0 \text{ mas yr}^{-1},\end{aligned}$$

where the associated error range is derived assuming that the observed region could have peculiar velocities of up to $\pm 10 \text{ km s}^{-1}$ (Stark & Brand 1989). We then conclude that the observed proper motions are roughly consistent with those expected for a source at the position of W3(OH).

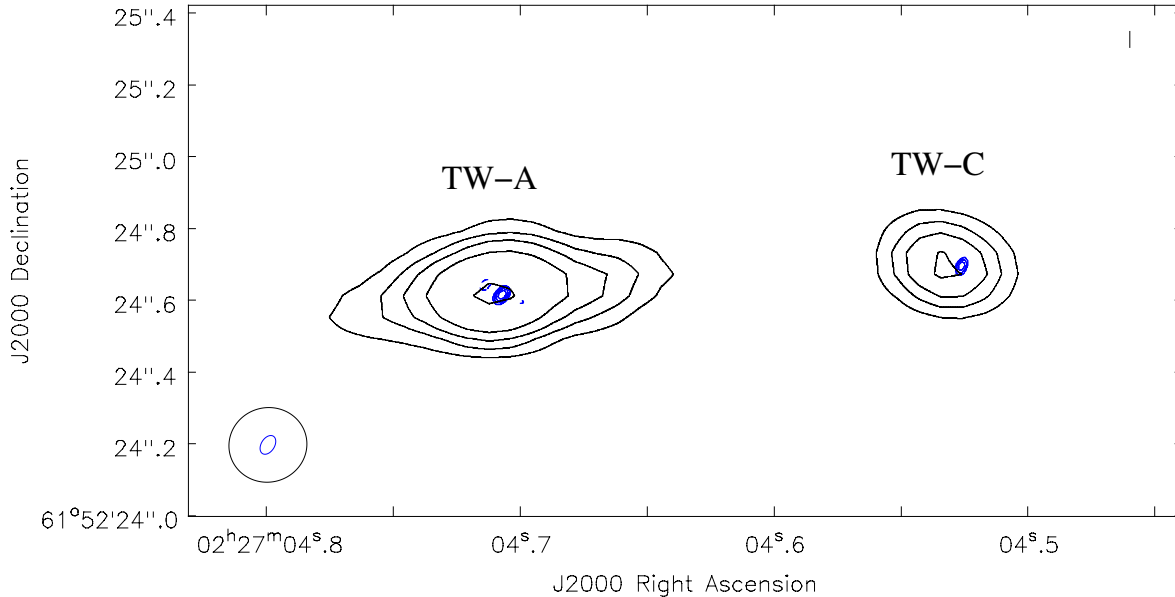


Fig. 5.— Image of the I Stokes parameter of the compact radio sources TW-A (left) and TW-C (right), given in blue contours, as detected in our Ka band (32.96 GHz) observations of epoch 2012.78. The contours are at -4 , 4 , 5 , 6 and 7 times the $1\text{-}\sigma$ noise level of $52 \mu\text{Jy beam}^{-1}$. The black contours delineate the 8.4 GHz emission from epoch 1996.19. The contours are at -4 , 4 , 8 , 12 , 18 , 36 times the $1\text{-}\sigma$ noise level of this region of the image ($15 \mu\text{Jy beam}^{-1}$). Note the small displacement in position for the peak emission between the two epochs. The half power contours of the 32.96 ($0''.057 \times 0''.037$; $PA = 148^\circ$) and 8.4 GHz synthesized beams ($0''.218 \times 0''.207$; $PA = 105^\circ$) are shown in the bottom left corner.

3.2. Counterparts at Other Wavelengths

At the epoch of the Kawamura & Masson (1998) indirect detection of the compact radio source there were no known counterparts at other wavelengths. More recent studies indicate the presence of counterparts at several wavelengths. A Class 0/I infrared young stellar object was detected by Rivera-Ingraham et al. (2011) at a position $\alpha(2000)=02^{\text{h}}27^{\text{m}}03^{\text{s}}86$, $\delta(2000)=61^{\circ}52'25''.32$. As they used Spitzer data we assume that their astrometric errors

are between $0''.35$ and $1''.0$ (Fadda et al. 2006). Thus, within positional errors, this infrared source coincides with the radio source.

We also searched in the 2MASS catalog (Cutri et al. 2003) and found a source, 2MASS 02270391+6152255, at an angular distance of $0''.5$ from the position of the radio source. Since the positional accuracy of the 2MASS survey, with respect to the International Celestial Reference System, is $0''.5$ (Skrutskie et al. 2006), we also consider this 2MASS source a counterpart to the compact radio source. However, since the star is enshrouded in an optically-thick shell ($\tau \sim 2.8$ at 37.1 microns, Hirsch et al. 2012) the emission observed with Spitzer and 2MASS is probably coming from the outer edge of this dust shell, at thousand to tens of thousands of AU from the star (Stecklum et al. 2002, Hirsch et al. 2012).

Feigelson & Townsley (2008) detected a hard X-ray source coincident within error with the compact radio source. In their words: *The young massive star ionizing W3(OH) is clearly detected in our Chandra observation, at $\alpha(2000)=02^{\text{h}}27^{\text{m}}03^{\text{s}}.84$, $\delta(2000)=61^{\circ}52'24''.9$. It is a surprisingly hard X-ray source; this hard emission allows it to be seen through a large absorbing column ($A_V \sim 75$ mag) inferred from the soft X-ray absorption.* Their positional error is $\sim 0''.4$.

Given that these sources detected in different surveys and at different wavelengths coincide within their positional errors with the compact radio source, we suggest that the latter is related with a very young massive stellar object projected inside the W3(OH) ultracompact H II, possibly its exciting star.

3.3. Similar Sources in the Literature

A previous detection of compact radio sources near the center of the HII regions NGC 6334E and NGC 6334A (both with shell morphologies) was reported by Carral et al. (2002). These compact sources were suggested to be associated with the exciting stars of the HII regions.

4. Interpretation

What is the nature of the compact radio source? Its positional coincidence with an embedded star, brightness temperature, spectral index and lack of circular polarization seem to favor a free-free emitting ionized stellar wind. There are, however, serious problems with this interpretation. Dzib et al. (2013) have tabulated the expected flux densities for ZAMS stars of different classes. The luminosity of W3(OH) ($7.1 \times 10^4 L_{\odot}$; Hirsch et al. 2012) and the rate of ionizing photons required to maintain its free-free emission of ~ 2 Jy in the optically-thin regime ($\sim 9 \times 10^{47} \text{ s}^{-1}$) can be provided by a B0V star, according to the tabulation of Dzib et al. (2013). For a B0V star located at a distance of 2.04 kpc, the expected flux density of its associated stellar wind at 22.64 GHz is only 0.006 mJy, about three orders of magnitude below the observed values. We note that the compact sources detected near the center of the HII regions NGC 6334(A) and NGC 6334(E) (Carral et al. 2002) are much brighter (by about two orders of magnitude) than the expected values for the O7.5 stars needed to ionize them. Furthermore, the compact radio source in W3(OH) shows strong time variation while the wind from a ZAMS star is expected to be steady. Finally, the observed width of the H58 α line suggests that we are observing an HII region or a photoevaporated wind, since much larger linewidths would be expected for a stellar wind.

Recent radio observations have shown time variability in HII regions on a timescale of

years (Franco-Hernández & Rodríguez 2004; Galván-Madrid et al. 2008). Franco-Hernández & Rodríguez (2004) proposed that the time variability may be due to changes in the source of the ionizing radiation, though it may also be due to increased absorption in the rapidly evolving core of the nebula. Peters et al. (2010a; 2010b), Galván-Madrid et al. (2011) and Klassen et al. (2012a; 2012b) have discussed theoretical scenarios that may account for the HII region variability. However, these observations and models address a situation in which the whole of the HII region changes. This does not seem to be the case for W3(OH), where the variation is restricted to the compact component while the whole of the nebula does not vary significantly (Kawamura & Masson 1998).

We tentatively propose that the compact radio source could be the result of either a slow shell ejection by the B0 star or by the passage of a dense gas clump that temporarily engulfs the star. In both cases we will have the dense gas close to the star that is required to explain the free-free emission. These possibilities, however, are rather *ad hoc*, and we explore the scenario of a photoevaporated disk, a fossil of the star formation process, around the exciting star of W3(OH). Using an expansion velocity of $\sim 4 \text{ km s}^{-1}$ for W3(OH) (Kawamura & Masson 1998) and a radius of 0.006 pc, W3(OH) has a kinematic age of only 1,500 years and the accretion disk that presumably existed around the star during its formation could still be present.

A compact ionized region around a young massive star can be produced by a photoevaporated disk (Hollenbach et al. 1994; hereafter H94). In the case of W3(OH) the compact source has a size of the order of 100 AU. This size corresponds to the gravitational radius $r_g = GM_*/a^2$ where M_* is the stellar mass and a is the sound speed of the ionized gas. Beyond this radius, the photoevaporated gas can escape from the potential well of the star. Inside r_g the gas is trapped and will form a static atmosphere that can produce the observed free-free emission.

As discussed above, the exciting source of W3(OH) has a luminosity $L_* \sim 7.1 \times 10^4 L_\odot$. According to Vacca, Garmany & Shull (1996), a ZAMS star with this luminosity has a stellar mass, $M_* \sim 19.5 M_\odot$, a stellar radius $R_* \sim 8.3 R_\odot$, and a rate of ionizing photons $\dot{N}_i \sim 1.44 \times 10^{48} \text{ s}^{-1}$. For this star, the gravitational radius is $r_g \sim 130 \text{ AU}$. The static atmosphere has an exponential electron number density profile $n_e(r, z) = n_0(r) \exp(-z^2/2H^2)$, as a function of height z and radius r , where $n_0(r)$ is the electron density at the disk surface and $H(r) = r_g(r/r_g)^{3/2}$ is the scale height. The number density $n_0(r)$ is given by eqn. (3.11) of H94, and one can obtain the free-free optical depth of a face-on disk as a function of radius, assuming an electron temperature of the ionized gas of $T_e \sim 6,500 \text{ K}$.

We find that the optical depth at 32.96 GHz decreases as a function of radius and becomes $\tau_{32.96\text{GHz}} \sim 1$ at $\theta \sim 0''.032$. The emission of the optically thick inner region is $\sim 13 \text{ mJy}$, close to the observed flux. The total emission of the static atmosphere up to $r_g \sim 130 \text{ AU}$ is $\sim 35 \text{ mJy}$, and we assume that the accretion disk has been truncated by the photoevaporation process beyond r_g . Furthermore, as shown in Figure 5 of Lugo & Lizano (2004), who modeled the photoevaporated disk wind in the source MWC 349A, the static atmosphere can produce a spectral index of the order of 1 for frequencies between 20 and 100 GHz. On the other hand, according to H94, to preserve the static atmosphere one requires a weak stellar wind because a strong wind would blow the static atmosphere up to a radius r_w where the ram pressure of the wind balances the thermal pressure of the ionized gas (see their Figure 1). For the case of W3(OH), the condition that $r_w < r_g$, imposes a condition on the stellar wind momentum $M_{w-6} v_{w8} < 7.5 \times 10^{-2}$ (eq. [4.3] of H94), where the stellar wind mass-loss rate M_{w-6} is normalized to $10^{-6} M_\odot \text{ yr}^{-1}$, and the stellar wind velocity v_{w8} is normalized to 1000 km s^{-1} . Therefore, this condition implies a critical value for the mass-loss rate, $\dot{M}_{\text{crit}} \sim 10^{-7} M_\odot \text{ yr}^{-1}$, which agrees with the value compiled by Dzib et al. (2013) for a B0 ZAMS star.

Finally, the flux variation on timescales of years, could be explained by a variation in the wind strength: if the wind momentum increases, it can blow away the static ionized atmosphere decreasing the observed radio flux. When the star returns to its low wind state, a static atmosphere will be regenerated and the flux will increase to its high value. Variations in the wind strength could be due to variations in the accretion rate through the disk as observed in young low-mass stars (e.g., Pech et al. 2010). In this scenario, sub-arcsecond sensitive millimetric observations should detect the dust emission from the fossil circumstellar disk that is being ionized by the central star.

5. Conclusions

In conclusion, the compact radio source projected near the center of W3(OH) coincides positionally with a massive young star and has brightness temperature, spectral index, and polarization characteristics suggestive of partially thick free-free emission. An interpretation in terms of an ionized stellar winds fails because of the large flux densities observed in the source. We tentatively propose that the compact radio source could be the result of either a slow shell ejection or the passage of a dense gas clump. Finally, we discuss a scenario where the emission originates in a static ionized atmosphere around a fossil photoevaporated disk.

S.A.D., L.F.R., S.E.K., L.L., S.L. and L.A.Z. are thankful for the support of DGAPA, UNAM, and of CONACyT (México). This research has made use of the SIMBAD database, operated at CDS, Strasbourg, France.

REFERENCES

- Brand, J., & Blitz, L. 1993, *A&A*, 275, 67L
- Carral, P., Kurtz, S. E., Rodríguez, L. F., et al. 2002, *AJ*, 123, 2574
- Cowie, L. L., Barger, A. J., Wang, W.-H., & Williams, J. P. 2009, *ApJ*, 697, L122
- Cutri, R. M., Skrutskie, M. F., van Dyk, S., et al. 2003, "The IRSA 2MASS All-Sky Point Source Catalog, NASA/IPAC Infrared Science Archive, <http://irsa.ipac.caltech.edu/applications/Gator/>"
- Dehnen, W., & Binney, J. J. 1998, *MNRAS*, 298, 387
- Dreher, J. W., & Welch, W. J. 1981, *ApJ*, 245, 857
- Dzib, S., Loinard, L., Rodríguez, L. F., Mioduszewski, A. J., & Torres, R. M. 2011, *ApJ*, 733, 71
- Dzib, S. A., Rodríguez, L. F., Loinard, L., et al. 2013, *ApJ*, 763, 139
- Fadda, D., Marleau, F. R., Storrie-Lombardi, L. J., et al. 2006, *AJ*, 131, 2859
- Feigelson, E. D., & Townsley, L. K. 2008, *ApJ*, 673, 354
- Franco-Hernández, R., & Rodríguez, L. F. 2004, *ApJ*, 604, L105
- Galván-Madrid, R., Rodríguez, L. F., Ho, P. T. P., & Keto, E. 2008, *ApJ*, 674, L33
- Galván-Madrid, R., Peters, T., Keto, E. R., et al. 2011, *MNRAS*, 416, 1033
- Gómez, L., Rodríguez, L. F., Loinard, L., et al. 2005, *ApJ*, 635, 1166
- Hachisuka, K., Brunthaler, A., Menten, K. M., et al. 2006, *ApJ*, 645, 337
- Hirsch, L., Adams, J. D., Herter, T. L., et al. 2012, *ApJ*, 757, 113

- Hollenbach, D., Johnstone, D., Lizano, S., & Shu, F. 1994, *ApJ*, 428, 654
- Kawamura, J. H., & Masson, C. R. 1998, *ApJ*, 509, 270
- Klassen, M., Pudritz, R. E., & Peters, T. 2012a, *MNRAS*, 421, 2861
- Klassen, M., Peters, T., & Pudritz, R. E. 2012b, *ApJ*, 758, 137
- Lugo, J., Lizano, S., & Garay, G. 2004, *ApJ*, 614, 807
- Pech, G., Loinard, L., Chandler, C. J., et al. 2010, *ApJ*, 712, 1403
- Peters, T., Banerjee, R., Klessen, R. S., et al. 2010a, *ApJ*, 711, 1017
- Peters, T., Mac Low, M.-M., Banerjee, R., Klessen, R. S., & Dullemond, C. P. 2010b, *ApJ*, 719, 831
- Reid, M. J., Argon, A. L., Masson, C. R., Menten, K. M., & Moran, J. M. 1995, *ApJ*, 443, 238
- Rivera-Ingraham, A., Martin, P. G., Polychroni, D., & Moore, T. J. T. 2011, *ApJ*, 743, 39
- Rodríguez, L. F., Zapata, L. A., & Ho, P. T. P. 2009, *ApJ*, 692, 162
- Sams, B. J., III, Moran, J. M., & Reid, M. J. 1996, *ApJ*, 459, 632
- Schönrich, R., Binney, J., & Dehnen, W. 2010, *MNRAS*, 403, 1829
- Schraml, J., & Mezger, P. G. 1969, *ApJ*, 156, 269
- Skrutskie, M. F., Cutri, R. M., Stiening, R., et al. 2006, *AJ*, 131, 1163
- Stark, A. A., & Brand, J. 1989, *ApJ*, 339, 763
- Stecklum, B., Brandl, B., Henning, T., et al. 2002, *A&A*, 392, 1025

- Torres, R. M., Loinard, L., Mioduszewski, A. J., et al. 2012, *ApJ*, 747, 18
- Turner, J. L., & Welch, W. J. 1984, *ApJ*, 287, L81
- Vacca, W. D., Garmany, C. D., & Shull, J. M. 1996, *ApJ*, 460, 914
- Wilner, D. J., Reid, M. J., & Menten, K. M. 1999, *ApJ*, 513, 775
- Wood, D. O. S., & Churchwell, E. 1989, *ApJS*, 69, 831
- Xu, Y., Reid, M. J., Zheng, X. W., & Menten, K. M. 2006, *Science*, 311, 54
- Zapata, L. A., Rodríguez-Garza, C., Rodríguez, L. F., Girart, J. M., & Chen, H.-R. 2011, *ApJ*, 740, L19